Low-temperature relaxor state induced by epitaxial compression in $PbSc_{0.5}Nb_{0.5}O_3$ films

M. Tyunina,[1,2] J. Levoska,[1] P.-E. Janolin,[3] and A. Dejneka[2]

[1]*Microelectronics and Materials Physics Laboratories, University of Oulu, P. O. Box 4500, FI-90014 Oulun yliopisto, Finland*

[2]*Institute of Physics, Academy of Sciences of the Czech Republic, Na Slovance 2, 182 21 Prague 8, Czech Republic*

[3]*Laboratoire Structures, Propriétés et Modélisation des Solides, Ecole Centrale Paris, 92290 Châtenay-Malabry, France*

(Received 4 April 2013; published 14 June 2013)

The use of high-performance perovskite-structure epitaxial relaxor ferroelectric films [S. H. Baek *et al.*, Science **334**, 958 (2011)] is hindered by the lack of knowledge of epitaxial effects therein. It is experimentally shown here that a biaxial epitaxial compression can favor the relaxor state over ferroelectricity. The absence of the ferroelectric transition and the existence of the low-temperature relaxor state are evidenced by a combination of x-ray diffraction, dielectric, polarization, and optical studies of $PbSc_{0.5}Nb_{0.5}O_3$ films epitaxially grown on $La_{0.5}Sr_{0.5}CoO_3$/MgO(001). This finding is beyond existing models of polarization in perovskite-structure epitaxial films and beyond the established ability to induce ferroelectricity by an epitaxial strain.

DOI: 10.1103/PhysRevB.87.224107 PACS number(s): 77.55.Px, 77.80.Jk, 77.80.bn, 77.55.fp

I. INTRODUCTION

Novel micro- and nanoelectronic devices enabled by the variety of electronic states and ferroic ordering in epitaxial films of perovskite-structure oxides are forming a rapidly growing area of research and development. Much attention is focused on future applications in morphic computational systems.[1] However, a broader trend in electronics is towards diversification, which requires a variety of compact sensing, actuating, and powering devices. As recently demonstrated,[2] epitaxial films of perovskite-structure relaxor ferroelectrics (RFEs) have an especially high potential for such devices. The dependence of properties of perovskite RFE films on epitaxial strain[3] becomes an issue of urgent practical importance.

Thus far, the influence of epitaxial strain on phase diagrams and properties is studied best for films of perovskite ferroelectrics (FEs), which have been extensively explored since the early 1990s.[4] In epitaxial FE films, the biaxial in-plane strain affects the polarization.[5] The strain-temperature phase diagrams of FE films have been calculated, and the appearance of new crystal and FE phases has been shown.[3,5] Moreover, a strain-induced onset of FE order has been predicted for films of non-FE materials. The strain-induced FE order in films of non-FE magnetic oxides attracts special interest due to possibility to create novel multiferroic magnetoelectrics. Thus, the concept of strain-induced FE order is well established today.[3]

Perovskite-structure RFEs are known to outperform normal FEs.[6,7] Huge electromechanical response, giant dielectric permittivity, strong pyroelectric, photovoltaic, electrocaloric, and other effects in RFEs[6,7] can enable advanced applications of epitaxial RFE films in a variety of fields including sensing, actuating, energy harvesting and storage, cooling, etc.[8–10] Indeed, the most remarkable electromechanical hyperactivity has been demonstrated in epitaxial films of RFE $PbMg_{1/3}Nb_{2/3}O_3$-$PbTiO_3$.[2] The wide use of RFE films is hindered by the lack of knowledge of effects produced by epitaxial strain on RFE properties.

The compositional complexity and insufficient fundamental understanding of RFEs make the theoretical analysis of epitaxial RFE films very difficult. The short-range order of polarization with a random orientation of local dipoles is widely accepted as the characteristic of relaxor (R) state.[6,7,11–13] The absence of polarization in the high-temperature paraelectric (PE) state and the long-range ordered polarization in the low-temperature FE state are characteristics of normal FEs. On cooling, bulk RFEs exhibit spontaneous structural and R-to-FE transitions (at a certain temperature T_s), while some relaxors, e.g. $PbMg_{1/3}Nb_{2/3}O_3$ (PMN), experience a gradual transformation to the low-temperature R state, without spontaneous FE transitions. Modern models of FEs predict strain-temperature phase diagrams containing the PE and the FE states, but they are unable to detect the R state thus far. The extrapolation of tendencies found in films of normal FEs to films of RFEs suggests that the epitaxial strain may favor new structural and FE phases and higher temperatures of the FE transitions in RFE films. Here, we demonstrate experimentally that the epitaxial strain can lead to the frustration of the spontaneous R-to-FE transition and to the formation of low-temperature R phases. This finding is beyond existing models of polarization and beyond the established ability to induce ferroelectricity by epitaxial strain. Novel relaxors and possibly relaxor-type magnetoelectrics with giant response functions may be created by controlling the epitaxial strain.

As the RFE material, we select $PbSc_{0.5}Nb_{0.5}O_3$ (PSN). In its bulk form, PSN experiences on cooling a cubic-to-rhombohedral structural phase transition and a simultaneous R-to-FE transition at $T_s \approx 380$–400 K. The temperature T_s depends on the degree of chemical rock-salt-type Sc:Nb ordering and the presence of dopants or defects.[14–20] It should be emphasized that obtaining the low-temperature R phase in bulk PSN by changing chemical ordering, concentration of defects and/or dopants is practically impossible.[14–20] Our experimental results evidence the low-temperature R phase in the epitaxial PSN film.

II. EXPERIMENT

Epitaxial heterostructures of perovskite PSN films were grown by pulsed laser deposition on top of $La_{0.5}Sr_{0.5}CoO_3$ (LSCO) bottom electrode layers and MgO (001) single-crystal substrates. During depositions, the substrate temperature was kept at 923 K. The pressure of high-purity ambient oxygen was

20 Pa during the deposition of LSCO. The oxygen pressure was increased to 80 Pa during the deposition of PSN to ensure proper lead and oxygen stoichiometry. The postdeposition cooling at a rate of $\sim$0.2 Ks^{-1} to room temperature was performed at an elevated oxygen pressure of 90 kPa. Dense stoichiometric targets of LSCO and PSN were prepared at the Institute of Solid State Physics, Riga, Latvia. For the electrical characterization of the PSN film, Pt/PSN/LSCO capacitors were formed. Circular Pt top electrodes (0.1, 0.2, and 0.4 mm^2 in area) were deposited using a shadow mask.

Scanning electron microscopy (SEM) was used for topographical imaging of the film surfaces and the heterostructure cross-sections and for the analysis of elemental composition of the films by energy dispersive x-ray spectroscopy (EDX/SEM). For determining chemical composition of the thin films, EDX spectra were acquired at different accelerating voltages and analyzed using standards and a STRATAGem software package.

The room-temperature crystal structure of the films was studied by x-ray diffraction (XRD) using Cu Kα radiation with a postmonochromator. The crystal orientation, perfection, epitaxy, and strain were analyzed using Θ-2Θ and ω-2Θ scans and ω rocking curves. The epitaxial relationship and chemical Sc:Nb ordering were also analyzed using ϕ scans carried out on a texture goniometer with β-filtered Cu Kα radiation. To confirm the in-plane epitaxy and to determine the lattice parameters of the films, the (004) reflections in Θ-2Θ scans and nonspecular (024) reflections were analyzed. The accuracy of lattice parameter determination was improved by using substrate reflections as a reference. The peak analysis included fitting of intensity by a sum of a background and peaks corresponding to the α_1 and α_2 lines of the Cu Kα radiation. The angular positions, intensities, and pseudo-Voigt shapes (widths and Gaussian/Lorentzian ratios) of the Cu Kα_1-Cu Kα_2 doublets were considered in the least-square fits. The lattice parameters were determined from the positions of the constituent peaks.

The temperature-dependent XRD measurements were carried out on a high-precision diffractometer using Cu Kα_1 radiation from an 18-kW rotating anode generator. The out-of-plane lattice parameters were refined from several Bragg reflections [namely: (00l), (002), (003), (004), (104), and (105)] at room temperature enabling the correction of a possible sample misalignment. The sample was then mounted in a cryostat and the (002) and (103) peaks were followed as a function of temperature. Their positions, together with the absolute reference at room temperature, were used to calculate the lattice parameters as a function of temperature. The positions of the peaks were optimized at each temperature. MgO (002) and LSCO (002) and (103) peak positions were determined similarly and cross-checked using tabulated data in order to ascertain the results on the thin films.

The dielectric properties were studied by measuring impedance $Z^* = R - iX$ of the formed capacitors. The measurements were carried out using an HP 4268A Precision LCR Meter and a Linkam TSE350 MultiProbe stage. For comparison and as a reference, thin-film capacitors of 260-nm-thick ferroelectric $Pb_{0.5}Sr_{0.5}TiO_3$ deposited on LSCO/MgO and with similar Pt top electrodes were used. Also as a reference, bulk capacitors in the form of circular platelets of disordered PSN ceramics with thickness $\sim$200 μm and with Ag electrodes were characterized. For the bulk PSN ceramic capacitors, an ideal capacitor approximation was considered, with the capacitance and the dielectric loss

$$C_s = \frac{1}{\omega X}, \tag{1}$$

$$\tan D = \frac{X}{R}, \tag{2}$$

where ω is the angular frequency $\omega = 2\pi f$. The thin-film capacitors were treated as leaky capacitors with the capacitance and the loss determined as

$$C_p = \frac{X}{\omega(X^2 + R^2)}, \tag{3}$$

$$\tan D = \frac{R}{X}, \tag{4}$$

The real part of the dielectric permittivity was calculated from the capacitance C_s or C_p considering parallel plate capacitors.

The dynamic polarization-electric field (P-E) and current-electric field (I-E) loops were recorded at different maximum applied voltages and different frequencies using aixACCT TF 1000 and TF 2000 Measurement Systems. The electric field E was calculated as $E = V/d$, where V is the applied voltage and d is the thickness of PSN.

The optical properties of the PSN films were studied by the method of variable-angle spectroscopic ellipsometry (VASE). A J. A. Woollam ellipsometer working in the range of photon energies 1–6.2 eV (wavelength $\lambda \sim$ 1200–200 nm) was used. The ellipsometric angles ψ and Δ were measured in the reflection mode at three angles of incidence (65°, 70°, and 75°) in order to construct an appropriate optical model. The measured spectra were analyzed using a WVASE32 software package considering the measured sample as a stack of semi-infinite substrate, homogenous film, surface roughness, and ambient air. The generalized multioscillator spectral model for the film was employed. The bare substrates, the substrates with the LSCO electrode layers, and the stacks with the PSN films were measured separately in order to decrease the number of fitting parameters and therefore accurately determine the optical constants of the PSN films. From the obtained absorption spectra, the region of the PSN transparency was found.

The temperature dependence of index of refraction $n(T)$ of PSN was determined using measurements at a fixed wavelength (600 nm) located in the transparency region of PSN. The cooling/heating runs were repeated several times and at different rates to ensure data reliability.

III. RESULTS

A. Epitaxial tetragonal PSN film

The cross-sectional SEM analysis shows the thickness of LSCO and PSN being $\sim$100 and $\sim$250 nm, respectively. EDX/SEM confirms the proper stoichiometry of the PSN films.

The room-temperature XRD analysis of PSN/LSCO/MgO shows that both the LSCO and perovskite PSN layers are highly oriented with (00l) planes parallel to the (001) surface of the MgO substrate [Fig. 1(a)]. No pyrochlore phase is detected in PSN. The in-plane orientations of the layers are revealed using ϕ scans through (022) and (112) reciprocal lattice

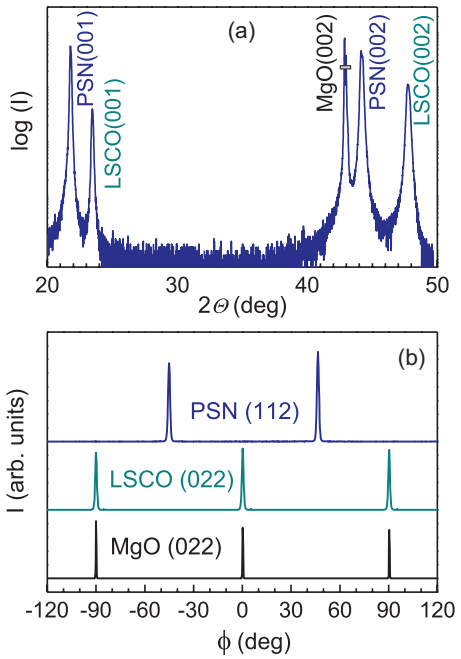

FIG. 1. (Color online) Crystal structure. Cu Kα radiation. (a) X-ray diffraction θ-2θ pattern of the PSN/LSCO/MgO heterostructure in the selected region around (001) and (002) reflections. The intensity of the substrate reflection is reduced by filtering (shown schematically). (b) In-plane epitaxy: ϕ scans through (022) and (112) reciprocal lattice points of MgO and LSCO, and PSN, correspondingly.

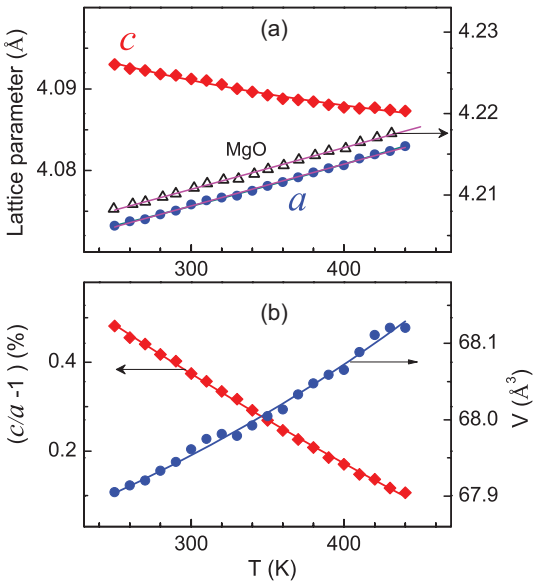

FIG. 2. (Color online) (a) The out-of-plane lattice parameter c (solid diamonds) and the in-plane lattice parameter a (solid circles) of the PSN film as a function of temperature. The lattice parameter of the cubic MgO substrate is also shown (open triangles). (b) The tetragonality ($c/a - 1$) and the unit cell volume V of the PSN film as a function of temperature.

points [Fig. 1(b)]. The epitaxial relationship is of cube-on-cube type PSN[100](001)‖LSCO[100](001)‖MgO[100](001). The inspection of ϕ scans through ($h + 0.5$, $k + 0.5$, $l + 0.5$) reciprocal lattice points of PSN shows intensity at superlattice reflections and hence some NaCl-type chemical Sc:Nb ordering.

The crystal structure of LSCO can be interpreted as tetragonal, with the measured room-temperature in-plane and out-of-plane lattice parameters $a_{\mathrm{LSCO}} \approx 3.864$ Å and $c_{\mathrm{LSCO}} \approx 3.805$ Å. Also the crystal structure of PSN can be interpreted as tetragonal, with the room-temperature in-plane and out-of-plane lattice parameters $a \approx 4.075$ Å and $c \approx 4.092$ Å, correspondingly. The lattice parameter of the perovskite-structure pseudocubic cell of bulk PSN is about $a_0 = 4.08(4)$ Å at room temperature.[15–17] The misfit strain in a pseudomorphic PSN film deposited on the LSCO layer grown on MgO ($a_{\mathrm{LSCO}} \approx 3.864$ Å) would be $s = (a_{\mathrm{LSCO}}/a_0 - 1) \times 100\% \approx -5.4\%$. The in-plane biaxial strain in the grown PSN film can be characterized by $s_{\mathrm{PSN}} = (a/a_0 - 1) \times 100\% \approx -0.2\%$, implying that the large PSN/LSCO misfit strain is efficiently relaxed. The relaxation of the misfit strain does not destroy the strong epitaxial film-substrate coupling as evidenced by the high perfection of the plane orientations: the full width at half maximum of the ω-rocking curves of (002) reflections are 0.65° for LSCO and 0.66° for PSN.

Investigations of the lattice parameters a and c as a function of temperature [Fig. 2(a)] reveal that the strain in PSN originates mainly due to mismatch between the coefficients of thermal expansion of the strongly coupled PSN film and MgO substrate. On cooling from 440 to 250 K, the in-plane lattice parameter a of the PSN film decreases linearly: $a \propto T$ [Fig. 2(a)]. The slope of the temperature dependence of $a(T)$ is about 5.1×10^{-5} K^{-1}, and it is equal to that of the linear temperature dependence of the lattice parameter of the cubic MgO substrate. The linear coefficient of thermal expansion of the PSN crystal is estimated using the data in Ref. 17, and it is about 2.4×10^{-6} K^{-1} (at 400 K), which is smaller than 12.1×10^{-6} K^{-1} (at 400 K) for the MgO substrate [Fig. 2(a)]. The decrease of the parameter a on cooling is dictated by the MgO substrate, and it leads to an increase of the out-of-plane parameter c of the PSN film, in agreement with the positive values of the elastic stiffness coefficients ($c_{11} > 2c_{12} > 0$). The grown PSN film has a metrically tetragonal crystal structure in the studied range of temperatures: $c > a$, with the room-temperature tetragonality ($c/a - 1$) being about 0.4%. In agreement with elastic properties of bulk PSN, the unit cell volume V in the PSN film shrinks: at room temperature, it is approximately equal to that of bulk PSN at hydrostatic pressure of ~1 GPa.[21]

The presence of a substrate-induced tetragonal crystal phase of PSN may be accompanied by a new structural and FE phase transition in the film compared to bulk. The results in Fig. 2 suggest the absence of structural transition at temperatures below 440 K. Further cooling to 100 K has not revealed any anomalies in the lattice symmetry and parameters that would be related to a phase transition. The dielectric response, polarization, and optical properties of PSN were investigated in order to identify the state of the film.

B. Dielectric response and polarization

The low-frequency dielectric response of the PSN film was studied as a function of temperature, frequency, and amplitude

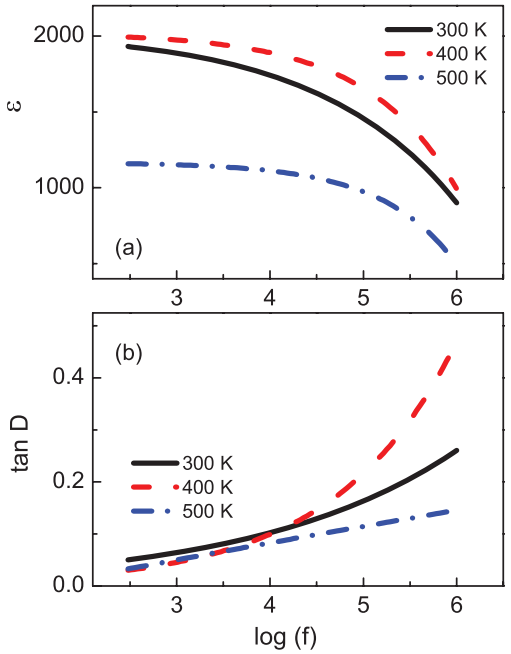

FIG. 3. (Color online) The apparent (a) real part ε of dielectric permittivity and (b) dielectric loss tan D as a function of frequency f at different temperatures in Pt/PSN/LSCO.

of the probing alternating electric field by measuring the impedance of Pt/PSN/LSCO capacitors. The impedance Z^* was analyzed using equivalent circuit modeling:[22]

$$Z^* = R_{EL} + \frac{R_F}{1+(\omega C_H R_F)^2} - i\frac{\omega C_H R_F^2}{1+(\omega C_H R_F)^2}, \quad (5)$$

where C_H is the heterostructure capacitance, R_{EL} is the resistance of thin-film electrodes, and R_F is the resistance of the RFE film determined mainly by its Ohmic resistance R_Ω, which is relatively small due to small thickness d of the film. The intrinsic frequency dispersion of the capacitance C_H in the case of the RFE films and three unknown parameters make it impossible to determine accurately the capacitance C_H using Eq. (5). The heterostructure capacitance can be roughly estimated as $C_H \approx C_p$ using Eq. (3) and considering $R_F \gg R_{EL}$. As seen from Eqs. (3)–(5), the estimated C_p and the measured loss factor are functions of frequency due to contributions of R_{EL} and R_Ω to the impedance Z^*. The relatively large R_{EL} can lead to apparent small C_p and large tan D at higher frequencies, and the relatively small R_Ω to large C_p and tan D at lower frequencies. These tendencies are seen in the Pt/PSN/LSCO capacitor (Figs. 3 and 4).

The apparent dielectric peak is broad, frequency dependent, and insensitive to the direction of temperature change (Fig. 4). Considering that the temperature dependences of resistances R_{EL} and R_Ω and of interfacial capacitance C_{INT} are negligible compared to the temperature dependence of the intrinsic capacitance C_F of the PSN film, and taking into account the results in Fig. 3, the temperatures T_m of the maxima in $\varepsilon(f,T)$ can be directly related to those in the PSN film for $f =$ 0.3–300 kHz.

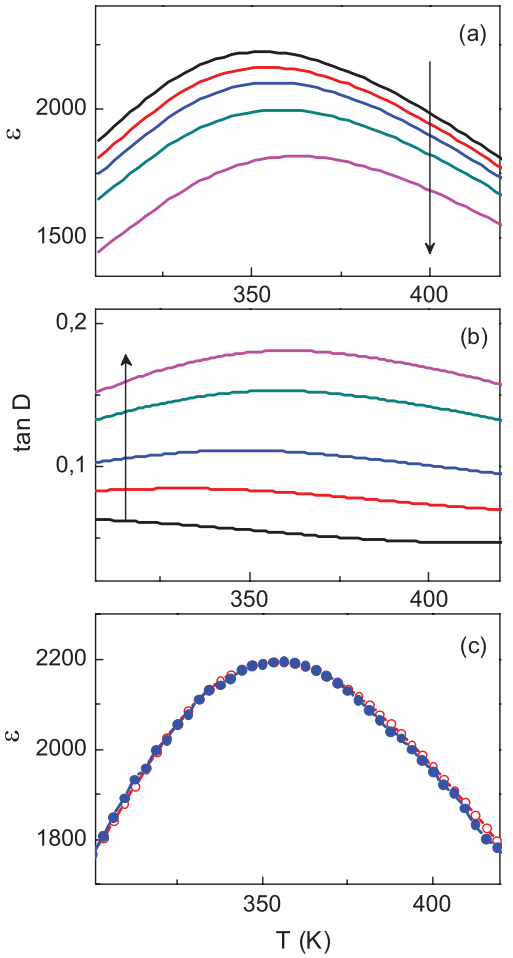

FIG. 4. (Color online) The apparent (a) and (c) dielectric permittivity ε and (b) loss tan D as a function of temperature T and (a) and (b) frequency $f = 0.3$–100 kHz in the Pt/PMN/LSCO. Arrows in (a) and (b) show the direction of frequency increase. Open and solid symbols in (c) show heating and cooling runs, correspondingly. $f =$ 1 kHz.

As an empirical proof of the RFE behavior, the Vogel-Fulcher relationship is widely accepted:

$$f = f_0 \exp\left[-\frac{T_A}{(T_m - T_f)}\right], \quad (6)$$

where f_0, T_A, and T_f are fitting parameters. The linear fit of $[1/(T_m - T_f)] \propto \ln(f)$ in Fig. 5 shows the validity of the Vogel-Fulcher relationship and evidences the RFE nature of the peak. Interestingly, the obtained fitting parameters $T_A \approx$ 46 K and $T_f \approx 347$ K in the studied PSN film are close to those in ceramic PSN at hydrostatic pressure of ~0.7 GPa.[23] This pressure correlates well with that suggested above considering the unit cell shrinkage.

The expected FE transition in the PSN film is difficult to assess directly using $\varepsilon(f,T)$. As previously evidenced, the FE transitions and the RFE behavior in thin films can be identified better from the temperature dependence of the derivative ξ of inverse permittivity:[22,24]

$$\xi(T) = \frac{\partial}{\partial T}\left(\frac{1}{\varepsilon}\right). \quad (7)$$

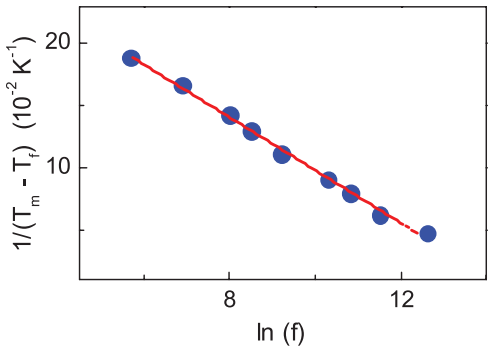

FIG. 5. (Color online) Dielectric properties. (a) The relationship between the temperature T_m of the dielectric maxima and the measurement frequency f. The straight line shows a fit to the Vogel-Fulcher law.

The shape of $\xi(T)$ in the PSN film (Fig. 6) is similar to that in epitaxial films of relaxor PMN.[24] The low-temperature Curie-Weiss behavior evidencing the FE state ($\xi = const < 0$) is well seen in the bulk ceramic PSN sample (measured for comparison) and in an epitaxial 260-nm-thick film of FE $Pb_{0.5}Sr_{0.5}TiO_3$ (PSTO).[22] On the contrary, indications of FE state are not found in the PSN film at low temperatures, by ~100 K lower than T_m. At such low temperatures, the FE state can be detected despite of smearing of $\xi(T)$, as it is illustrated in the PSTO film. The derivative analysis for the PSN film evidences the PMN-like behavior, without the FE transition.

The low-temperature PMN-like R state in the PSN film is confirmed by studies of the nonlinear dynamic dielectric

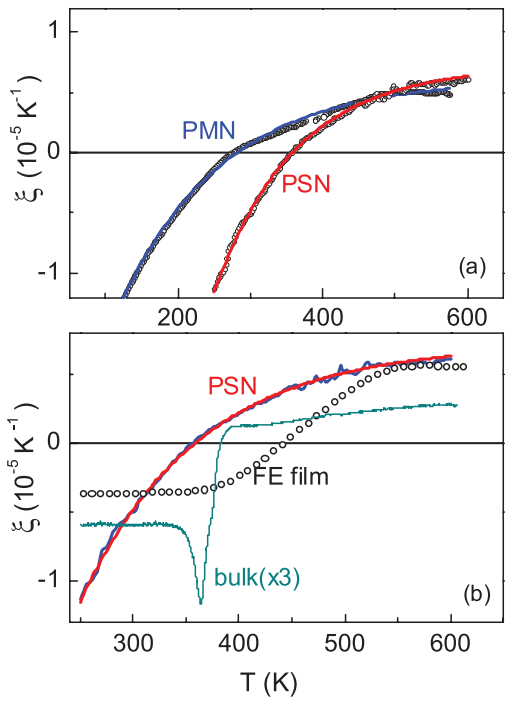

FIG. 6. (Color online) Derivative ξ of inverse permittivity as a function of temperature determined at $f = 10$ kHz in the PSN film in comparison with that in (a) the epitaxial PMN film[24] and in (b) the bulk PSN ceramic (dashed line, data reduced by factor 3) and the FE $Pb_{0.5}Sr_{0.5}TiO_3$ film (open circles).[22] Lines are smoothed data.

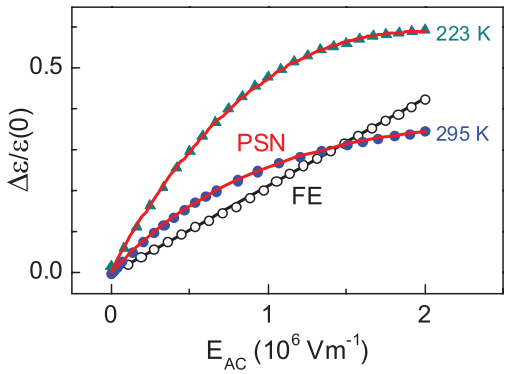

FIG. 7. (Color online) Normalized change $\Delta\varepsilon/\varepsilon(0)$ of the dielectric permittivity as a function of amplitude E_{AC} of ac electric field determined at $f = 10$ kHz in the PSN film. Lines are third-order polynomial fits. For comparison also $\Delta\varepsilon/\varepsilon(0)$ in the 260-nm-thick FE $Pb_{0.5}Sr_{0.5}TiO_3$ film and a linear fit are shown.[27]

response. With increasing amplitude E_{AC} of the sinusoidal alternating electric field, the dielectric permittivity is known to increase both in the R state and in the FE state. The dependence $\varepsilon(E_{AC})$ in the R state is related to the dynamics of polar clusters, and it can be presented as a polynomial of E_{AC}.[25] On the contrary, the dependence $\varepsilon(E_{AC})$ in the FE state is related to the motion of FE domain walls, and it is usually described by the Rayleigh-type law $\varepsilon \propto E_{AC}$.[26] The normalized change of permittivity is defined as

$$\frac{\Delta\varepsilon}{\varepsilon(0)} = \frac{\varepsilon - \varepsilon(0)}{\varepsilon(0)}, \tag{8}$$

where $\varepsilon(0)$ is the extrapolated permittivity at $E_{AC} = 0$. It is a polynomial of E_{AC} in the R state and a linear function of E_{AC} in the FE state.

The plots of $\Delta\varepsilon/\varepsilon(0)$ versus E_{AC} (Fig. 7) determined in the PSN film at $T = 295$ K (i.e. by ~60 K below T_m) and $T = 223$ K (i.e. by ~130 K below T_m) can be fitted well by third-order polynomials. For comparison, a linear dependence $\Delta\varepsilon/\varepsilon(0) \propto E_{AC}$ is found in the FE PSTO film at $T = 393$ K (i.e. by 50 K below T_m).[27] The results in Fig. 7 confirm the low-temperature R state and the absence of a low-temperature FE state in the PSN film.

The R state in the PSN film is also evidenced by slim dynamic polarization-electric field (P-E) loops [Fig. 8(a)]. With increasing maximum applied field, the loops evolve from those typical for leaky linear dielectric to those of leaky nonlinear dielectric. The Rayleigh-type internal loops, typical for FEs, are not observed. The apparent coercive field E_C (corresponding to $P = 0$ in the dynamic loops) increases strongly with increasing frequency [Fig. 8(b)]. This is in contrast to the behavior in FEs. On cooling, the apparent field E_C grows, but the non-FE character of the loops remains unchanged.

C. Optical properties

The low-temperature R state in the epitaxial tetragonal PSN film is further proven by studies of optical properties. As previously shown,[28,29] intrinsic FE phase transitions in thin films can be identified from the temperature evolution of the optical index of refraction $n(T)$ determined at photon energies

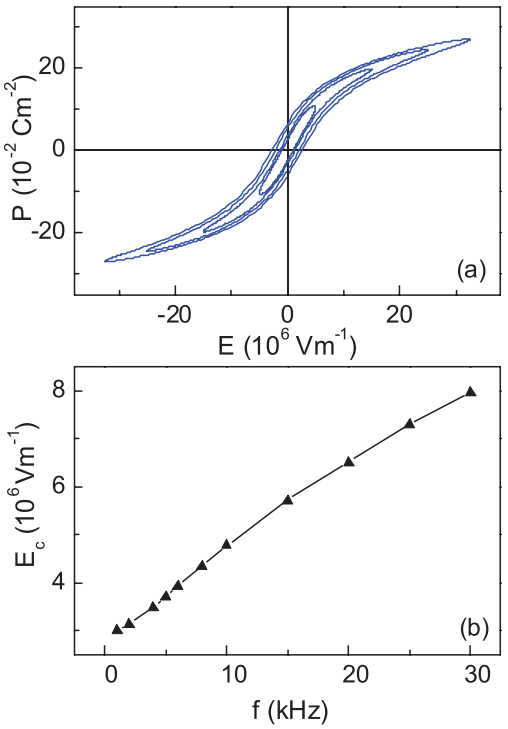

FIG. 8. (Color online) (a) The room-temperature dynamic polarization-electric field (P-E) loops in Pt/PSN/LSCO recorded at different maximum applied voltages and $f = 1$ kHz. (b) The apparent coercive field E_C as a function of frequency f at maximum applied field of 37.5 $\times$ 10^6 Vm^{-1}.

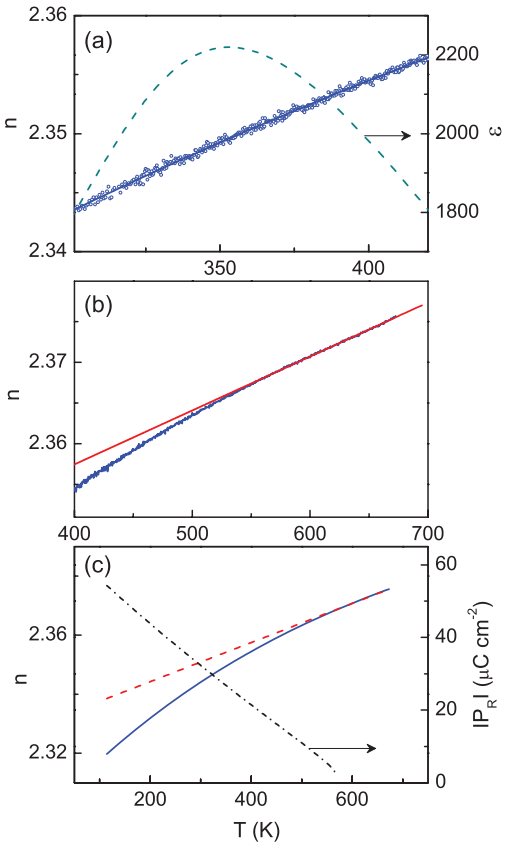

FIG. 9. (Color online) Index of refraction n as a function of temperature (wavelength 600 nm). In (a), line shows smoothed data. Dashed line shows the dielectric permittivity ε (f = 1 kHz). The high-temperature linear fits $n_l(T)$ are shown by straight lines in (b) and (c). Dotted line in (c) shows estimated average random polarization $|P_R|$.

in the transparency range of the film. The FE transitions are manifested by a change of slope of $n(T)$ and a decrease of n on cooling in thin films. The behavior is qualitatively similar to that in crystals,[30,31] although $n(T)$ is more gently sloping in thin films. The RFE crystals exhibit on cooling a smooth deviation of $n(T)$ from the linear high-temperature behavior ($n \propto T$), with the spontaneous R-to-FE transition seen as a drop of n.[32–38]

The dependence $n(T)$ determined in the PSN film (Fig. 9) does not exhibit anomalies that could be associated with an FE transition. In contrast to the peak in $\varepsilon(T)$ around $T_m \approx$ 350–370 K, the index $n(T)$ decreases smoothly on cooling without any detectable extrema or deflection points in the range of temperatures T = 300–450 K [Fig. 9(a)]. The high-temperature $n(T)$ in the PSN film can be approximated by a line at $T >$ 560 K [Fig. 9(b)]:

$$n_l(T) \approx 2.33 - 6.62 \times 10^{-5} T. \quad (9)$$

The deviation δn of the index of refraction from the extrapolated linear dependence is commonly ascribed to the appearance of a randomly oriented polarization:

$$\delta n = n(T) - n_l(T), \quad (10)$$

$$\delta n = -\tfrac{1}{2} n_l^3 \cdot g \cdot |P_R|^2, \quad (11)$$

where g is the electro-optic coefficient and $|P_R|$ is the average random polarization.[39] The polarization $|P_R|$ is estimated assuming $g = 0.01$ m^{4}C^2 and using the experimentally found n_l and δn.[40] The estimated $|P_R|$ grows on cooling below 560 K [Fig. 9(c)]. Assuming that the deviation of $n(T)$ from the linear high-temperature behavior may be considered as an anomaly associated with FE transition, the PSN film would be FE below 560 K. The dynamic polarization and the dielectric response evidence the absence of FE state below 560 K. The dependencies $n(T)$ and $|P_R|(T)$ confirm the PMN-like R state in the PSN film.

IV. DISCUSSION

The self-consistent experimental results evidence that the spontaneous R-to-FE transition and the low-temperature FE phase existing in bulk PSN are absent in the epitaxial PSN film with metrically tetragonal crystal structure. As emphasized earlier, the low-temperature FE phase in bulk PSN is stable: it is practically impossible to eliminate it by changing chemical ordering or concentration of defects and/or dopants.[14–20]

The observed R phase cannot be explained in the frame of existing models. However, it is known that, in bulk PSN, the FE transition can vanish at moderate hydrostatic pressures around 1 GPa.[23,41–43] The unit cell volume and the Vogel-Fulcher fitting parameters in the PSN film are found to correspond to those in bulk PSN at hydrostatic pressure of about 1 GPa.[21,23] These observations allow us to suggest that the state of the epitaxial PSN film may be compared to the

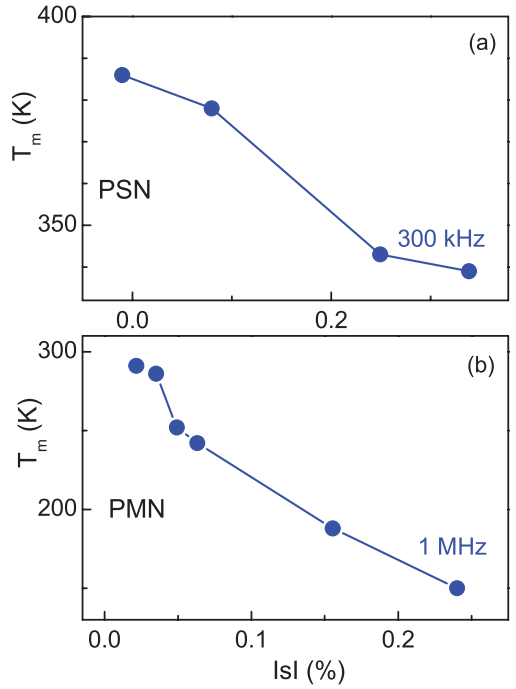

FIG. 10. (Color online) The temperature T_m of the dielectric maxima as a function of magnitude $|s|$ of the in-plane biaxial strain in epitaxial films of (a) PSN and (b) PMN.[24,44]

pressure-induced state in bulk PSN. Although the two-dimensional compression of the film is not mechanically equivalent to the three-dimensional compression under hydrostatic pressure, the in-plane decrease of interatomic distances in the film may lead to new atomic displacements. The effect may resemble that caused by lattice shrinkage under pressure.[42] The biaxial epitaxial compression can induce relaxor behavior in a way resembling the action of a moderate hydrostatic pressure.

The suggested role of epitaxial compression is supported by the behavior of epitaxial PSN and PMN films where the magnitude of epitaxial compression has been varied by varying deposition conditions or film thickness.[24,44,45] With increasing magnitude $|s|$ of the biaxial in-plane compressive strain, the temperatures T_m shift to lower temperatures (Fig. 10). This shift is opposite to the theoretically expected increase of phase transition temperatures in perovskite FE films,[10] and it agrees well with the lowering of T_m in bulk PMN and PSN under elevated hydrostatic pressure.[43]

V. CONCLUSIONS

Epitaxial perovskite PSN films with a metrically tetragonal crystal structure and a biaxial in-plane compressive strain are grown on LSCO/MgO(001). The combination of x-ray diffraction, dielectric, polarization, and optical studies evidences the absence of ferroelectric transition in PSN. The low-temperature relaxor state found in PSN is beyond existing models of polarization in epitaxial perovskite films. It is ascribed to the action of epitaxial compression resembling that of a moderate hydrostatic pressure. The observed effect opens possibilities to control the relaxor state. To understand the phenomena is a challenge.

ACKNOWLEDGMENTS

The research has been supported by the Academy of Finland (Project No. 264961), GACR (Grant No. P108/12/1941), Agence Nationale de la Recherche (Project ANR-11-BS10-016-02), and through ERA.Net (Project STP-133).

[1]S. D. Ha and S. Ramanathan, J. Appl. Phys. **110**, 071101 (2011).
[2]S. H. Baek, J. Park, D. M. Kim, V. A. Aksyuk, R.R. Das, S. D. Bu, D. A. Felker, J. Lettieri, V. Vaithyanathan, S. S. N. Bharadwaja, N. Bassiri-Gharb, Y. B. Chen, H. P. Sun, C. M. Folkman, H. W. Jang, D. J. Kreft, S. K. Streiffer, R. Ramesh, X. Q. Pan, S. Trolier-McKinstry, D. G. Schlom, M. S. Rzchowski, R. H. Blick, and C. B. Eom, Science **334**, 958 (2011).
[3]For review see J. M. Rondinelli and N. A. Spaldin, Adv. Mater. **23**, 3363 (2011).
[4]For review see D. G. Schlom, L. Q. Chen, C. B. Eom, K. M. Rabe, S. K. Streiffer, and J. M. Triscone, Ann. Rev. Mater. Res. **37**, 589 (2007).
[5]N. A. Pertsev, A. G. Zembilgotov, and A. K. Tagantsev, Phys. Rev. Lett. **80**, 1988 (1998).
[6]G. A. Smolenskii, V. A. Bokov, V. A. Isupov, N. N. Krainik, R. E. Pasynkov, and A. I. Sokolov, *Ferroelectrics and Related Materials* (Gordon and Breach, New York, 1984).
[7]Z. G. Ye (ed.), *Handbook of Advanced Dielectric, Piezoelectric and Ferroelectric Materials—Synthesis, Properties and Applications* (Woodhead Publishing Ltd., Cambridge, UK, 2008), p. 1096.
[8]C. Hofer, M. Hoffmann, U. Boettger, and R. Waser, Ferroelectrics **270**, 179 (2002).
[9]R.W. Whatmore and R. Watton, Ferroelectrics **236**, 259 (2000).
[10]C. B. Eom and S. Trolier-McKinstry, MRS Bull. **37**, 1007 (2012).
[11]R. Blinc, J. Dolinšek, A. Gregorovič, B. Zalar, C. Filipič, Z. Kutnjak, A. Levstik, and R. Pirc, Phys. Rev. Lett. **83**, 424 (1999).
[12]S. B. Vakhrushev, A. A. Naberezhnov, N. M. Okuneva, and B. N. Savenko, Phys. Solid State **37**, 1993 (1995).
[13]G. Xu, J. Wen, C. Stock, ans P.M. Gehring, Nat. Mater. **7**, 562 (2008), and references therein.
[14]F. Chu, I. M. Reaney, and N. Setter, J. Appl. Phys. **77**, 1671 (1995).
[15]C. Malibert, B. Dkhil, J. M. Kiat, D. Durand, J. F. Berar, and A. Spasojevic-de Bire, J. Phys.: Condens. Matter **9**, 7485 (1997).
[16]C. Perrin, N. Menguy, E. Suard, Ch. Muller, C. Caranoni, and A. Stepanov, J. Phys.: Condens. Matter **12**, 7523 (2000).
[17]K. G. Abdulvakhidov, I. V. Mardasova, T. P. Myasnikova,V. A. Kogan, R. I. Spinko, and M. F. Kupriyanov, Phys. Solid State **43**, 508 (2001).
[18]O. Bidault, C. Perrin, C. Caranoni, and N. Menguy, J. Appl. Phys. **90**, 4115 (2001).

[19]I. P. Raevskii, V. V. Eremkin, V. G. Smotrakov, E. S. Gagarina, and M. A. Malitskaya, Phys. Solid State **42**, 161 (2000).
[20]C. Perrin, N. Menguy, O. Bidault, C. Y. Zahra, A. M. Zahra, C. Caranoni, B. Hilczer, and A. Stepanov, J. Phys.: Condens. Matter **13**, 10231 (2001).
[21]M. Ahart, H. K. Mao, R. E. Cohen, R. J. Hemley,G. A. Samara, Y. Bing, Z. G. Ye, and S. Kojima, J. Appl. Phys. **107**, 074110 (2010).
[22]M. Tyunina, M. Plekh, M. Antonova, and A. Kalvane, Phys. Rev. B **84**, 224105 (2011).
[23]M. Szafranski, A. Hilczer, and W. Nawrocik, J. Phys.:Condens. Matter **16**, 7025 (2004).
[24]M. Tyunina, M. Plekh, and J. Levoska, Phys. Rev. B **79**, 054105 (2009).
[25]R. Pirc, R. Blinc, and V. Bobnar, Phys. Rev. B **63**, 054203 (2001).
[26]N. Bassiri-Gharb, I. Fujii, E. Hong, S. Trolier-McKinstry, D. V. Taylor, and D. Damjanovic, J. Electroceram. **19**, 47 (2007).
[27]M. Tyunina, L. Yao, M. Plekh, J. Levoska, and S. van Dijken, Adv. Funct. Mater. **23**, 467 (2013).
[28]M. Tyunina, J. Narkilahti, M. Plekh, R. Oja, R. M. Nieminen, A. Dejneka, and V. Trepakov, Phys. Rev. Lett. **104**, 227601 (2010).
[29]M. Tyunina, A. Dejneka, D. Chvostova, J. Levoska, M. Plekh, and L. Jastrabik, Phys. Rev. B **86**, 224105 (2012).
[30]W. J. Merz, Phys. Rev. **76**, 1221 (1949).
[31]W. Kleemann, F. J. Schafer, and D. Rytz, Phys. Rev. B **34**, 7873 (1986).
[32]E. Wiesendanger, Ferroelectrics **1**, 141 (1970).
[33]O. Yu. Korshunov, P. A. Markovin, and R. V. Pisarev, Ferroelectrics Letters **13**, 137 (1992).
[34]G. Burns and B. A. Scott, Solid State Commun. **13**, 423 (1973).
[35]G. Burns and F. H. Dacol, Solid State Commun. **42**, 9 (1982).
[36]W. Kleemann, F. J. Schafer, and M. D. Fontana, Phys. Rev. B **30**, 1148 (1984).
[37]A. S. Bhalla, R. Guo, L. E. Cross, G. Burns, F. H. Dacol, and R. R. Neurgaonkar, Phys. Rev. B **36**, 2030 (1987).
[38]P. A. Markovin, W. Kleemann, R. Lindner, V. V. Lemanov, O. Yu. Korshunov, and P. P. Syrnikov, J. Phys.: Condens. Matter **8**, 2377 (1996).
[39]A. W. Smith, G. Burns, B. A. Scott, and H. D. Edmonds, J. Appl. Phys. **42**, 684 (1971).
[40]The coefficient is unknown and assumed to be close to that in PMN.
[41]E. L. Venturini, R. K. Grubbs, G. A. Samara, Y. Bing, and Z. G. Ye, Phys. Rev. B **74**, 064108 (2006).
[42]B. J. Maier, N. Waeselmann, B. Mihailova, R. J. Angel, C. Ederer, C. Paulmann, M. Gospodinov, A. Friedrich, and U. Bismayer, Phys. Rev. B **84**, 174104 (2011).
[43]G. A. Samara and E. L. Venturini, Phase Transitions **79**, 21 (2006).
[44]J. Levoska and M. Tyunina, Ferroelecrics **291**, 11 (2003).
[45]M. Tyunina, J. Levoska, and S. Leppävuori, J. Appl. Phys. **91**, 9277 (2002).